ROR1 sustains multivesicular endosomes by interacting with HRS and STAM1

Tomoya Yamaguchi (tyamaguchi@kumamoto-u.ac.jp)
Kumamoto University https://orcid.org/0000-0001-6933-543X
Masatoshi Yamamoto
Kumamoto University
Masaya Yamazaki
Kumamoto University
Naoki Tani
Kumamoto University
Mai Sakamoto
Kumamoto University
Hina Daikuzono
Kumamoto University
Hao Li
Kumamoto University
Chitose Oneyama
Aichi Cancer Center Research Institute https://orcid.org/0000-0002-5719-9431
Toyoshi Fujimoto
Juntendo University https://orcid.org/0000-0002-3601-7977
Takashi Takahashi
Aichi Cancer Center Research Institute

Article

Keywords: ROR1, caveolae formation, caveolae-dependent endocytosis, caveolae components, pro-survival signaling, HRS, STAM1, ESCRT-0

Posted Date: August 24th, 2020

DOI: https://doi.org/10.21203/rs.3.rs-52722/v1

ROR1 sustains multivesicular endosomes by interacting with HRS and STAM1

Tomoya Yamaguchi[1,2,7], Masatoshi Yamamoto[1], Masaya Yamazaki[1], Naoki Tani[3], Mai Sakamoto[1], Hina Daikuzono[1], Hao Li[1], Chitose Oneyama[2,4], Toyoshi Fujimoto[5], Takashi Takahashi[6]

[1]Department of Cancer Biology, Graduate School of Medical Sciences, Kumamoto University, Kumamoto 860-8556, Japan

[2]JST, PRESTO, Saitama, 332-0012, Japan

[3]Liaison Laboratory Research Promotion Center, Institute of Molecular Embryology and Genetics, Kumamoto University, Kumamoto 860-0811, Japan

[4]Division of Cancer Cell Regulation, Aichi Cancer Center Research Institute, Nagoya 464-8681, Japan

[5]Laboratory of Molecular Cell Biology, Research Institute for Diseases of Old Age, Juntendo University Graduate School of Medicine, Tokyo, 113-8421, Japan

[6]Aichi Cancer Center Research Institute, Nagoya 464-8681, Japan

[7]Correspondence and requests for materials should be addressed to T.Y. (email: tyamaguchi@kumamoto-u.ac.jp).

ABSTRACT

The receptor tyrosine kinase-like orphan receptor 1 (ROR1) regulates caveolae formation and caveolae-dependent endocytosis by interacting with caveolae components, which in turn sustains pro-survival signaling toward AKT from multiple RTKs, including EGFR, and MET. We report here a novel function of ROR1 as a scaffold for HRS and STAM1, two essential components of ESCRT-0. The present results show that ROR1 facilitates interactions of HRS and STAM1, thereby preventing the lysosomal degradation of HRS. Furthermore, interaction of ROR1 with STAM1 was found to be required to sustain binding of ROR1 to HRS as well as HRS subcellular localization. Additionally, ROR1 localized in both the limiting membrane and intraluminal vesicles (ILVs) of Rab5-induced multivesicular endosomes (MVEs) containing HRS, CD63, and EEA1 was found to regulate the formation of Rab5-induced MVEs by an association with the GTP-bound form of Rab5 in cancer cells. Notably, ROR1 depletion inhibits CD63-positive MVEs formation and reduces exosomes release. Our findings provide the first evidence that the onco-embryonic antigen receptor ROR1 regulates exosome biogenesis via MVE formation in cancer cells.

INTRODUCTION

Endosomes have critical roles in the highly dynamic transport mechanism that operates between the plasma membrane and lysosomes via the biosynthetic secretory pathway[1, 2, 3]. Early endosomes mature into late endosomes then accumulate intraluminal vesicles (ILVs) in the lumen, and are thereafter referred to as multivesicular endosomes (MVEs) or multivesicular body (MVBs)[4, 5, 6, 7]. ILVs formed by inward budding of early endosomal membrane sequester proteins, lipids, and cytosol are specifically sorted. In most cells, the main fate of MVBs is to fuse with lysosomes for degradation of their contents, while an alternative function is exocytic fusion with the plasma membrane leading to release of ILVs as exosomes into extracellular space[8, 9]. Exosomes are generally defined as secreted extracellular vesicles (EVs) and known to play key roles in cell-to-cell communication[10, 11]. However, knowledge regarding the mechanisms that control the alternative fates of ILVs to degradation or secretion is largely unknown. Thus, an important unanswered question is how are MVBs that fuse with lysosomes different from those that fuse with the plasma membrane to release exosomes, which the present study attempted to address.

The endosomal sorting complexes required for transport (ESCRT) components involved in MVB and ILV biogenesis[12, 13]. This is an intricate protein machinery composed of four separate protein ESCRTs (-0, -I, -II, -III) that function cooperatively to facilitate MVE formation, vesicle budding, and protein cargo sorting[14]. ESCRT-0, -I, and -II contain ubiquitin-binding subunits that function to sort ubiquitylated membrane proteins to specific domains of endosomes and into endosomal invaginations, while ESCRT-III subsequently drives vesicle scission[15]. ESCRT-0 contains HRS (hepatocyte growth factor-regulated tyrosine kinase substrate, gene symbol *HGS*), which recognizes monoubiquitinated cargo proteins and is associated with STAM (signal transducing adaptor molecule, another ESCRT-0 component)[12]. Evidence is accumulating indicating that sorting of proteins into ILVs can

also occur in a manner independent of ubiquitination. The transferrin receptor (TfR) in reticulocytes generally undergoes exosome secretion, though does not become ubiquitylated[16]. It has also been shown that ALIX is involved in exosome biogenesis and exosomal sorting of syndecans in a manner independent of ubiquitin[17]. However, some studies have found that the ESCRT-0 members HRS and STAM are required for exosome secretion, as demonstrated by decreased exosome secretion following HRS or STAM inhibition in various cell types[18, 19, 20, 21]. Since exosomes correspond to ILVs, the same mechanisms are thought to be involved in their biogenesis. Nevertheless, the precise details regarding MVE/MVB formation for exosomes remain unclear.

We previously reported that the receptor tyrosine kinase (RTK)-like orphan receptor 1 (ROR1) is a transcriptional target of the lineage-survival oncogene NKX2-1/TTF-1 in lung adenocarcinomas[22, 23]. In addition to its kinase-dependent role, ROR1 serves as a scaffold protein to facilitate interaction between CAV1 and CAVIN1, and consequently maintains caveolae formation in lung adenocarcinoma cells, which in turn sustains pro-survival signaling toward AKT from multiple RTKs, including EGFR and MET[24]. Therefore, ROR1 is an attractive target for overcoming EGFR-TKI resistance caused by various mechanisms such as EGFR double mutation and bypass signaling from other RTKs. Recently, we also showed that ROR1 has a novel scaffold function that is vital for efficient caveolae-dependent endocytosis[25]. CAVIN3 was demonstrated to bind with ROR1 at a site distinct from site for CAV1 and CAVIN1, a function necessary for proper subcellular localization of CAVIN3 and caveolae-dependent endocytosis. Additionally, evidence demonstrating a mechanistic link of ROR1-CAVIN3 interaction and consequential caveolae trafficking with RTK-mediated pro-survival signaling towards AKT in early endosomes was obtained.

The present findings revealed a novel function of ROR1 as a scaffold for HRS and STAM1. ROR1 was shown to facilitate interactions of HRS and STAM1, thereby preventing

lysosomal degradation of HRS. Furthermore, we also found that interaction of ROR1 with STAM1 is required to sustain binding of ROR1 to HRS as well as HRS subcellular localization. Together, these results show that ROR1 regulates formation of Rab5-induced MVEs by an association with the GTP-bound form of Rab5. Additionally, ROR1 depletion inhibits CD63-positive MVEs formation and reduces exosome release in cancer cells.

RESULTS

ROR1 knockdown reduced HRS and STAM1 proteins, and altered late endosome localization.

Based on our previous results showing that ROR1 sustains caveolae formation and caveolae-dependent endocytosis[24, 25], we speculated that ROR1 may be involved in cell membrane organization and dynamics in cancer cells. Initially, we analyzed the effects of siROR1 treatment on membrane dynamics and trafficking using electron microscopy, which revealed a large number of abnormal vesicles in the cytoplasm of NCI-H1975 cells (Fig. 1a). Thus, we examined whether ROR1 was required for Golgi or ESCRT protein. Western blot (WB) analysis revealed significantly decreased expressions of HRS and STAM1 proteins, but not of TGN38 or GM130, in siROR1-treated NCI-H1975 cells (Fig. 1b), after which siROR1-induced reduction of HRS and STAM1 was confirmed in three lung cancer cell lines, NCI-H1975, PC-9, and SK-LC-5 (Fig. 1c). Following siROR1 transfection, HRS expression was decreased, while that of STAM1 gradually decreased though remained readily detectable for up to 24 hours (Fig. 1d). These findings led us to speculate that abnormal vesicles in cytoplasm induced by siROR1 may be caused by impairment of the ESCRT-0 machinery. Consistent with previous investigations[4, 26, 27], HRS- and STAM1-depleted cells showed typically large and ring-shaped vacuoles with one or two intralumenal vesicles, similar to that seen in NCI-H1975 cells following ROR1 knockdown (Supplementary Fig. 1). We also found that the subcellular localization of Rab7 (late endosome marker) and CD63 (exosome marker) was markedly altered in siROR1-treated cells (Fig. 1e and 1f). The present findings clearly indicate that ROR1 is required to sustain HRS and STAM1 expression, as well as resultant proper endosome formation in cancer cells.

Identification of HRS and STAM1 as ROR1-binding proteins

To gain more in-depth insight regarding the involvement of ROR1 in this process, we next investigated whether ROR1 interacts with HRS and/or STAM1. Immunoprecipitation-western blotting (IP-WB) analysis using octylglucoside[28] as a detergent revealed an interaction of endogenous ROR1 with endogenous HRS and STAM1 in PC-9 and NCI-H1975 lung cancer cells (Fig. 2a). IP-WB analysis using A549 cells transfected with an ROR1-GFP expression vector verified interactions of ROR1 with endogenous HRS and STAM1 (Fig. 2b). Pull-down assay findings obtained using purified glutathione S-transferase (GST)-tagged ROR1 protein as well as lysates of NCI-H1975 cells also demonstrated an interaction of ROR1 with HRS or STAM1 (Fig. 2c). Additionally, immunofluorescence analysis revealed partial colocalization of punctate signals of ROR1-GFP with those of HRS and STAM1 (Fig. 2d).

ROR1 localized in both the limiting membrane and ILVs of Rab5-induced MVEs

To determine whether ROR1 is present in MVEs, we used the constitutively active mutant $Rab5^{Q79L}$, which is known to induce formation of enlarged early endosomes by promotion of their homotypic fusion[29]. As expected, co-expression of mCherry-$Rab5^{Q79L}$ with ROR1-GFP resulted in the presence of both proteins in enlarged early endosomes. Furthermore, ROR1-GFP was found colocalized with HRS, CD63, and EEA1 (Fig. 3a and Supplementary Fig. 2). In addition, partial colocalization of ROR1-GFP and mCherry-$Rab5^{Q79L}$ was verified at a much higher resolution in super-resolution structured illumination microscopy (SIM)[30] findings (Fig. 3b), while line intensity profiles of individual endosomes clearly showed ROR1 localization in the lumen and membrane of Rab5-induced endosomes (Fig. 3c). Electron microscopy was also employed and confirmed those immunofluorescence data, with the presence of ROR1-GFP showing an association with both the limiting membrane and ILVs of Rab5-induced MVEs in immunoelectron microscopy analysis (Fig. 3d). An ascorbate peroxidase (APEX2) system was then employed to better visualize the presence of ROR1 in

MVEs, as APEX2 has improved enzyme activity for biotinylating proteins within 20 nm and can increase electron microscopy contrast by catalyzing 3,3′-diaminobenzidine (DAB) polymerization[31, 32, 33]. Biotinylated proteins were predominantly detected in ROR1-APEX2-expressed HeLa cells (Supplementary Fig. 3a), with those results confirmed by WB analysis with a streptavidin-horseradish peroxided (HRP) process (Supplementary Fig. 3b). ROR1-APEX2 was clearly localized in both the limiting membrane and ILVs of endogenous MVEs, findings consistent with our immunofluorescence results (Fig. 3e).

ROR1 required for prevention of HRS being routed to lysosomes

HRS and STAM become stabilized by forming a complex via their coiled-coil regions and HRS-STAM interaction is required to prevent degradation of each protein[34, 35]. Interaction of HRS with STAM leads to ESCRT-0, which has a crucial role for initiation of the ESCRT pathway[36]. Therefore, we performed ROR1 knockdown and examined its effect on the interaction between HRS and STAM1 by taking advantage of the delayed reduction of HRS and STAM1 that occurs after siROR1 transfection. A significantly decreased association of HRS with STAM1 was observed in PC-9 and NCI-H1975 cells at 24 hours after siROR1 treatment (Fig. 4a). In addition, subcellular localization of HRS was markedly altered at that time point, resulting in significant colocalization with the endosome/lysosome marker LAMP1 (Fig. 4b). These findings indicated that ROR1 has a novel function as an indispensable scaffold protein of HRS and STAM1, thus preventing lysosomal HRS degradation and sustaining HRS expression.

ROR1-STAM1 interaction required for HRS-STAM1 binding and HRS subcellular localization

An interesting finding was inhibition of the interaction of ROR1 with HRS in NCI-H1975

cells caused by STAM1 knockdown at 24 hours after siSTAM1 transfection under conditions that did not have effects on HRS expression (Fig. 5a). Consistent with that result, two-color immunofluorescence analysis revealed significant loss of ROR1-GFP and HRS colocalization (Fig. 5b). Next, we used various ROR1 deletion mutants to examine the STAM1 binding regions. IP-WB analysis revealed a requirement of the C-terminal proline-rich domain of ROR1 for its binding to STAM1 (Fig. 5c). We also investigated whether the STAM1-binding region of ROR1 has effects on formation of an HRS and STAM1 complex, and/or HRS subcellular localization. NCI-H1975 cells stably reconstituted with either siRNA-resistant ROR1-WTm or ROR1-ΔPm were subjected to treatment with siROR1, then IP-WB analysis was performed. Different than ROR1-WTm, STAM1-binding deficient ROR1-ΔPm did not sustain the interaction of HRS with STAM1 (Fig. 5d). On the other hand, similar to treatment with siROR1, HRS subcellular localization was altered in ROR1-ΔPm-expressing cells, resulting in colocalization of HRS with LAMP-1 (Fig. 5e). These results indicate a requirement of the STAM1-binding region of ROR1 to sustain the interaction of ROR1 with HRS, as well as stabilize the HRS protein for prevention of being routed to lysosomes.

Rab5 identified as ROR1-HRS and ROR1-STAM1 binding protein

To further evaluate the interaction of ROR1 with HRS/STAM1 and its function, a split-APEX2 system[37] was used by taking advantage of ROR1 binding with HRS or STAM1. ROR1-AP, HRS-EX and STAM-EX fragments are inactive on their own, though are reconstituted to provide peroxidase activity when driven together by a molecular interaction (Fig. 6a and Supplementary Fig. 4a). The split-APEX2 system enables biotin labelling on proteins that are located within 20 nm from active reconstituted APEX2. Biotinylated proteins are then affinity-enriched with streptavidin beads, with the eluted products analyzed by mass spectrometry (LC-MS/MS). Fluorescence analysis results showed that V5-tagged ROR1-AP

and HA-tagged HRS-EX or STAM1-EX complexes formed puncta, and were tightly co-localized with biotinylated proteins (Fig. 6b and Supplementary Fig. 4b). Using WB analysis with streptavidin-HRP, H_2O_2- and APEX2-dependent biotinylation of protein complexes surrounding ROR1-HRS or ROR1-STAM1 interactions were confirmed (Fig. 6c and Supplementary Fig. 4c). Biotinylated proteins are enriched by streptavidin selection and can be analyzed with LC-MS/MS. Among the proteins which were detected only in ROR1-AP+HRS-EX or ROR1-AP+STAM1-EX, RAB5A and RAB5B were identified as ROR1/HRS and ROR1/STAM1 binding proteins, respectively (Fig. 6d, Supplementary Fig. 4d, and Supplementary Table 1). Evidence obtained in previous studies strongly suggests that HRS is recruited to endosomes[12, 36]. In the present study, a proximity ligation assay (PLA) was performed to detect protein-protein interactions in close proximity (<40 nm)[38, 39], which revealed a significant foci of signals arising from ROR1-GFP and endogenous HRS in the proximity of the membrane of mCherry-Rab5^{Q79L}-expressed endosomes (Fig. 6e). These results indicate recruitment of HRS to Rab5-positive early endosomes by ROR1.

ROR1 required for formation of Rab5-induced MVEs

Rab5^{Q79L} causes formation of enlarged endosomes (MVEs) that have a large number of ILVs, while those containing both early and late endocytic markers are also frequently observed[29, 40]. To investigate the role of ROR1 in MVEs in greater detail, the effects of siROR1 treatment on Rab5-induced MVE formation were subjected to analysis. Interestingly, Rab5^{Q79L}-induced MVE enlargement was reduced by ROR1 knockdown (Fig. 7a and 7b). Furthermore, in siROR1-treated HeLa cells, small sized-Rab5^{Q79L} MVEs were surrounded by lysosomes (Fig. 7c). The Rab5^{Q79L} mutant has been shown to stimulate fusion between endosomes and is known to more active because of its low GTPase activity, causing a higher proportion to be in a GTP-bound state, which leads to increased fusion of early endosomes and results in

oversized MVEs[29, 40]. We found that the amount of GTP-bound Rab5 was significantly decreased in ROR1-depleted cells (Fig. 7d). Also, IP-WB analysis revealed an interaction of ROR1 with the $Rab5^{Q79L}$ form, but not the $Rab5^{WT}$ form (Fig. 7e). These results indicate that ROR1 interacts with and stabilizes GTP-bound Rab5, which then sustains Rab5-induced MVE formation.

ROR1 depletion inhibits CD63-positive MVEs formation and reduces exosome release

Findings obtained in the present experiments led us to speculate that the HRS/STAM1/Rab5 interacting function of ROR1 might also be involved in exosome biogenesis via formation of MVEs in cancer cells, thus we investigated MVE formation. Using immunoelectron microscopy, localization of CD63, an exosome marker, was examined in cells knocked down for ROR1. In contrast to CD63 labelling observed in typical MVE structures in siControl-treated cells, few CD63 labels were found in the vestige of MVE in siROR1-treated cells (Fig. 8a), suggesting ROR1 to be essential for formation of CD63-positive MVEs in cancer cells. In addition, ROR1 was found in isolated exosomes in amounts proportional to the amount of ROR1 expression in cells from which the exosomes were derived (Fig. 8b). We also examined exosomes from lung cancer cells using nanoparticle tracking analysis (NTA). Consistent with previously reported findings[18, 19, 20, 21], exosome secretion was significantly decreased in HRS- as well as STAM1-depleted NCI-H1975 lung cancer cells. However, it was interesting to note that while inhibition of ROR1 did not have an effect on exosome size, siROR1-treated NCI-H1975 lung cancer cells also showed reduced exosome secretion (Fig. 8c and Supplementary Fig. 5). Together, the present findings clearly show that ROR1 facilitates the interaction of HRS with STAM1 in Rab5-induced MVE membranes of cancer cells, which results in sustained MVE formation and exosome secretion via its scaffold function for HRS and STAM1 (Fig. 8d).

DISCUSSION

The present study revealed an unanticipated function of ROR1, an onco-embryonic antigen receptor present in cancer cells. ROR1 was shown to have a role as a scaffold protein for HRS and STAM1, and facilitate their association in the membranes of Rab5-induced early endosomes. That interaction of ROR1 with STAM1 was found to maintain HRS expression by preventing lysosome-dependent degradation. Also, ROR1 regulates Rab5 as well as subsequent MVE formation, which in turn is involved in exosome biogenesis in cancer cells.

Generally, lysosomal targeting of signaling receptors is controlled by sorting via HRS/STAM and their downstream partners for membrane invagination in early endosomal regions, which become MVEs[12]. Subsequently, ILVs are transported to lysosomes where they are degraded along with receptors in their possession. However, several details about exosomes remain unknown, including how MVBs destined for exocytosis are different from those destined for transport to lysosomes. A recent study showed that tumor cell exosomes contain syndecan, syntenin, and ALIX, and that exosome biogenesis is dependent on ESCRT function[8, 17]. In other studies, HRS was demonstrated to be linked to exosome secretion by showing reduced exosome amounts released from HRS-deficient dendric cells or HRS-depleted HEK293 cells, and tumor cells[18, 19, 20]. The present findings provide clear evidence showing involvement of ROR1 in sustainment of exosome biogenesis through MVE formation in an ESCRT-dependent manner in lung cancer cell lines as well as HeLa cells, which suggests various mechanisms of exosome secretion under different cellular physiological states.

In the present study, ROR1 was shown required to sustain MVE formation via the interaction of HRS and STAM1 in cancer cells. It is possible that ROR1 is involved in formation of MVEs in various fetal tissues including the lungs, which have abundant ROR1 expression, because ROR1 functions as an onco-embryonic antigen[41, 42]. However, we

consider it unlikely that ROR1 is invariably required for stabilization of HRS and STAM1 expression, because of its negligible level or absence of expression in normal human adult tissues[41, 42]. In this regard, UBPy (USP8) is essential for stability of the HRS-STAM complex in MEF cells[43], which do not express ROR1. As for the existence of marked tissue-type specificity related to HRS and STAM expression, there may be distinct molecular mechanisms involved in sustainment of MVE formation for some cell states or lineage, which might potentially have effects on the function of MVEs.

In the present investigation, electron microscopy revealed that ROR1 knockdown resulted in a marked number of abnormal vesicles in cytoplasm of lung cancer cells. It is also notable that this specific morphological impairment was repeated by knockdown of HRS or STAM1. Previous studies showed that *S. cerevisiae* and *D. melanogaster* mutants have an impaired Hrs function, as well as a reduced number of ILVs in endosomes and vacuoles[6, 44], and that the same effect can be reproduced in mammalian cells treated with siHRS[26]. Also, siHRS-treated HeLa cells show typically large and ring-shaped vacuoles, and contain few internal vesicles[26]. Our study obtained similar results with NCI-H1975 lung cancer cells treated with siRNA against ROR1, suggesting that ROR1 might be indirectly responsible for intralumenal vesicle formation by initiating recruitment of HRS and STAM1 to endosome membranes, and also indicate that ROR1 controls not only controls MVE formation but also generation of ILVs in cancer cells. Furthermore, lipid microdomains and their components may be involved in ILV generation, or function together with other proteins with an affinity for lipid raft domains[45]. Our previous study showed a portion of ROR1 residing in detergent-resistant membranes (DRMs) that contained the caveolae-specific protein CAV1, consequently ROR1 is considered responsible for maintaining formation of caveolae and also caveolae-dependent endocytosis in lung cancer cells[24]. Therefore, we speculate that high amounts of ROR1 in exosomes indicate that recruitment of other membrane proteins from the limited membranes

of endosomes into ILVs of MVBs is involved in their early incorporation into ROR1-containing DRM domains.

HRS overexpression is known to be associated with malignancy and poor prognosis[5, 46], and previous studies shown an association of several types of human cancer, such as colorectal, gastric, and hepatocellular carcinomas, with a significantly elevated expression of HRS[47, 48], though the underlying related molecular mechanism remains unclear. Additionally, HRS-deficient mice, or mice with double knockout of STAM1 and STAM2 show embryonic mortality[49, 50]. HRS and STAM1 are not likely to serve as suitable molecular targets for cancer therapy due to their crucial physiological functions in various normal organs. In this regard, it is important to note that ROR1 is an onco-embryonic antigen showing tumor-specific expression in adults[41, 42]. As a result, the scaffold function of ROR1 is an attractive target for dealing with tumor-specific exosome secretion in cancer cells. In the present study, we found ROR1 expression in exosomes from lung cancer cells, which led us to speculate that ROR1-positive exosomes may have crucial roles in tumor progression, metastasis, signaling transduction, and/or tumor-to-stroma communication. These are exciting area for future research. Finally, ROR1 is suggested to play important roles in development of lung cancer as well as other types of human malignancy, including that in the breast[51], pancreas[52], stomach[53], colon[52], ovary[54], and skin[41], and also acute and chronic leukemia[42, 55, 56, 57].

In summary, ROR1 was found to possess an unanticipated function as a scaffold protein of HRS and STAM1, and thus sustains MVEs formation and exosome secretion from cancer cells. Future investigations of ROR1 functions are needed to elucidate the molecular mechanisms involved in regulation of cancer cell membrane dynamics and trafficking.

METHODS

Cell lines

The derivation, characteristics, and culture conditions of the human lung adenocarcinoma cell lines (NCI-H1975, PC-9, SK-LC-5) utilized, and the immortalized human lung epithelial cell line HPL1D were previously reported[22]. HeLa cells were purchased from Japanese Collection of Research Bioresources Cell Bank. All cell lines were authenticated by short tandem repeat (STR) DNA profiling and were free of mycoplasma contamination.

Reagents and antibodies

Duolink In Situ Starter Set FAR RED (DUO92001, DUO92005, DUO92013, DUO82049), (+)-Sodium L-ascorbate (#A7631), and Trolox (#238813) were purchased from Sigma-Aldrich (St. Louis, MO). Biotin Phenol (Biotinyl tyramide, #CDX-B0270-M100) were purchased from AdipoGen Life Sciences (San Diego, CA). NeutrAvidin coated magnetic beads (TAS8848 N1171) were purchased from Tamagawa Seiki (Nagano, Japan). HRP conjugated Streptavidin (#S911), DyLight-405 labeled NeutrAvidin (#22831), and pRc/CMV plasmid vector (V75020) were purchased from Thermo Fisher scientific (Waltham, MA). In-Fusion HD Cloning Kit was purchased from Takara-Bio (Shiga, Japan). mito-V5-APEX2 (#72480), NLS-MCP-AP_pLX304 (# 120918), and EX-HA-FRB-Cb5_pLX304 (# 120915) were a gift from Alice Ting and mCherry-Rab5^{Q79L} (#35138) was a gift from Sergio Grinstein via Addgene (Watertown, MA).

Anti-ROR1 (#16540/rabbit), anti-HRS (#15087/rabbit), anti-CAV1 (#3267/rabbit), anti-STAM1 (#13053/rabbit), anti-RAB5 (#3540/rabbit), anti-RAB7 (#9367/rabbit) antibodies were purchased from Cell Signaling Technology (Beverly, MA), while anti-LAMP1 (sc-20011/mouse) antibody from SantaCruz (Santa Cruz, CA), anti-GM130 (PM061/rabbit) antibody from MBL (Nagoya, Japan), anti-TGN38 (2F7-1/mouse) antibody from Novus

Biologicals (Littleton, CL), anti-EEA1 (610456/mouse) antibody from BD Bioscience (Bedford, MA), anti-CAVIN1 (ab135655/rabbit) antibody from Abcam (Cambridge, MA), anti-V5 (M167-3/mouse) antibody from Medical & Biological Laboratories (Nagoya, Japan), anti-GFP (mFX73, 012-20461) and anti-CD63 (#012-27063 for WB) antibodies from Wako Pure Chemical (Osaka, Japan). Anti-β-Actin (#A1978/mouse) and anti-β-tubulin (#T9026/mouse) were purchased from Sigma-Aldrich (St. Louis, MO). Anti-CD63 (for IF) CD9 (602.29 cl. 11) were kindly gifted from August, J.T. / Hildreth, J.E.K. and Anti- Andrews, P.W., respectively via Developmental Studies Hybridoma Bank (Iowa City, IA), while anti-mouse IgG (#7076) and anti-rabbit IgG (#7074) from Cell Signaling Technology.

Primers

The following primers were used to construct various ROR1 mutants by *in vitro* mutagenesis:

5’-CGGTCCTGGGAGGGACTCTCAAGTC-3’, ROR1-TKΔ1-F;

5’-AGCAGAAAGAGGTAGCTCTTTAGCC-3’, ROR1-TKΔ1-R;

5’-ATCATGAGATCCCCACACTCTGATG-3’, ROR1-TKΔ2-F;

5’-GAGGAACTCATGGAGATCCCCCTGA-3’, ROR1-TKΔ2-R;

5’-ATTCGCTGGATGCCCCCTGAAGCCA-3’, ROR1-TKΔ3-F;

5’-GGGCAGCAAGGACTTACTCTGGACC-3’, ROR1-TKΔ3-R;

5’-AACCCCAGATATCCTAATTACATGT-3’, ROR1-ΔST1-F;

5’-CCGAAGCCGGACGTGAATATCTTTA-3’, ROR1-ΔST1-R;

5’-AAGAGTCGGTCCCCAAGCAGTGCCA-3’, ROR1-ΔP-F;

5’-GTTACTGAGATTACTCACTGGGCTG-3’, ROR1-ΔP-R;

5’-AATCAGGAAGCAAATATTCCTTTAC-3’, ROR1-ΔST2-F;

5’-CTTGGGAGGTGGGCAGTGCTGAATC-3’, ROR1-ΔST2-R.

The following primers were used to construct various split-APEX2 vectors by In-Fusion

cloning techniques:

5’- GGATCCAAGGGCTCGGGCTC -3’, AP-pLX304-F;

5’- CATGGTTCTATCTCCTTCGAAG -3’, AP-pLX304-R;

5’- GGAGATAGAACCATGCACCGGCCGCGCCGC-3’, ROR1-AP-F;

5’- CGAGCCCTTGGATCCCAGTTCTGCAGAAATCATAG-3’, ROR1-AP-R;

5’- AAGGGCTCGGGCTCGACCTC -3’, EX-pLX304-F;

5’- CATGGTTCTATCTCCTTCGAAG -3’, EX-pLX304-R;

5’- GGAGATAGAACCATGGGGCGAGGCAGCGGCACC -3’, HRS-EX-F;

5’- CGAGCCCGAGCCCTTGTCGAATGAAATGAGCTGG -3’, HRS-EX-R;

5’- GACGCCTAACTGCAGCTGCCTCCCCTGGAGCGC -3’, EX-STOP-F;

5’- CTGCAGTTAGGCGTCGGCAAATCCCAGTTCTG -3’, EX-STOP-R;

5′ - GGAGATAGAACCATGCCTCTTTTTGCCACCAATC -3′, STAM-EX-F;

5′ - CGAGCCCGAGCCCTTTAGCAGAGCCTTCTGAGAA -3′, STAM-EX-R;

The following primers were used to construct ROR1-APEX2 vectors:

5′ - ATCATCTAGAGGCAAGCCCATCCCCAAC -3′, Xba1-V5-APEX2-F;

5′ - TGATGGGCCCTTAGGCATCAGCAAACCC -3′, APEX2-Stop-Apa1-R;

5′ - ATCAAAGGTTCCACCATGCACCGGCCGCGC -3′, Hind3-ccacc-ROR1-F;

5′ - ACGTTCTAGACAGTTCTGCAGAAATCATAG -3′, ROR1(-Stop)-Xba1-R.

siRNAs

The following RNA oligomers were obtained from QIAGEN (Hilden, Germany), and used for RNA interference:

5’-CAGCAATGGATGGAATTTCAA-3’, siROR1 (SI00071295),

5’-CACGTCCGGAGTAACACTACA-3’, siHRS (SI00067305),

5’-CAGCAATGATTAAGAACCTTA-3’, siSTAM1 (SI00734447).

siControl (AllStars Negative Control siRNA) was also obtained from QIAGEN.

Constructs

Constructions of pCMVpuro-ROR1 was previously reported[22]. Based on the pCMVpuro-ROR1 vector, pCMVpuro-ROR1-TKΔ1 (Δ473-564), pCMVpuro-ROR1-TKΔ2 (Δ564-655), pCMVpuro-ROR1-TKΔ3 (Δ655-746), pCMVpuro-ROR1-ΔST1 (Δ748-782), pCMVpuro-ROR1-ΔP (Δ784-861), and pCMVpuro-ROR1-ΔST2 (Δ853-876) were prepared by *in vitro* mutagenesis using KOD -Plus- DNA polymerase (TOYOBO) according to the manufacturer's instructions. pCMVpuro-ROR1-WTm and pCMVpuro-ROR1-ΔPm carrying multiple silent mutations at the binding site of siROR1 were constructed by *in vitro* mutagenesis using KOD -Plus- DNA Polymerase (TOYOBO) and the oligonucleotide primer 5'-CAACAGTGGACAGAGTTCCAG-3' (mutated residues are underlined). GFP-tagged ROR1 was constructed using Gateway system (Invitrogen) according to the manufacturer's instructions. The entire open reading frames of the resultant constructs were thoroughly sequenced.

To construct ROR1-AP_pLX304 vector, the ORF of ROR1 was amplified with the primers ROR1-AP-F and ROR1-AP-R containing the 15 bp region of homology to the NLS-MCP-AP_pLX304 vector. The NLS-MCP-AP_pLX304 vector also amplified except for the NLS region using AP-pLX304-F and AP-pLX304-R primers by PCR. These PCR products were gel purified and mixed with 1:1 molar ratio and incubated with In-Fusion HD reaction enzyme at 50 °C for 15 min, according to the instruction manual. Following incubation, the mixture was transformed into Stbl2 Competent Cells (NEB), and recombinant clones were selected on LB agar plates supplemented with Ampicillin at 30°C. Like this process, HRS or STAM1 ORF sequence recombined with the EX-HA-FRB-Cb5_pLX304 vector to construct the HRS-EX_pLX304 or STAM1-EX_pLX304 vector.

To construct ROR1-APEX2 vector, full-length of APEX2 was amplified with the primers Xba1-V5-APEX2 Fw and APEX2-Stop-Apa1. The amplified DNA fragment was digested with *XbaI* and *ApaI* and introduced into the pRC/CMV vector (pRC/CMV-APEX2). Full-length of ROR1 was amplified with the primers Hind3-ccacc-ROR1 Fw and Rv ROR1(-Stop)-Xba1. The amplified DNA fragment was digested with *HindIII* and *XbaI* and introduced into the pRC/CMV-APEX2 vector (pRC/CMV-ROR1-APEX2).

RNA interference

Cells were seeded at $5.0x10^4$ cells per well in 12-well plates with coverslip for immunofluorescence microscopy; at $1.0x10^5$ per well in 6-well plates for WB analysis and electron and immunoelectron microscopy; and at $1x10^6$ in 10 cm dishes for IP-WB analysis. On the next day, the cells were transfected with siRNAs (each at 20 nM) using Lipofectamine RNAiMAX (Invitrogen), according to the manufacturer's instructions. The cells were fixed or harvested 48 hr for immunofluorescence analysis or 72 hr for WB or IP-WB analysis after transfection. In the IP-WB analysis of the interaction between HRS and STAM1 or ROR1 and HRS in siROR1 or siSTAM1-treated cells respectively, the cells were harvested 24 hr after siRNA transfection. In the time course analysis, the cells were harvested or fixed at indicated time points after siROR1 or siControl transfection for WB analysis.

WB and IP-WB analyses

WB and IP-WB analyses were performed according to standard procedures using Immobilon-P filters (Millipore) and an enhanced chemiluminescence system (GE Healthcare). To analyze the physical interactions between ROR1 and HRS or STAM1, as well as those between HRS and STAM1, whole-cell lysates of NSCLC cell lines were solubilized in octylglucoside buffer (60 mM octylglucoside, 150 mM NaCl and 50 mM EDTA) and immunoprecipitated with anti-

ROR1, anti-HRS, or non-specific IgG antibodies. For determining the interacting region of ROR1 with STAM1, various ROR1 expression constructs were transfected into COS-7 cells. The cells were harvested 24hr after transfection with the NP-40 lysis buffer containing 20 mM Tris-HCl (pH 8.0), 137 mM NaCl, 2 mM EDTA, 1% NP-40, 10% Glycerol and 1 mM Na_3VO_4 and a complete EDTA-free protease inhibitor mixture (Roche). To examine the interactions between ROR1 and $Rab5^{WT}$ or $Rab5^{Q79L}$, Rab5 mutants-transfected Hela cells were solubilized in octylglucoside buffer and immunoprecipitated with anti-ROR1, or non-specific IgG antibodies.

Clarification of ROR1-RNAi effects

Stable transfectants expressing siRNA-resistant forms of ROR1-WT or ROR1-ΔP were generated by introducing the respective plasmids (pCMVpuro-ROR1-WTm or pCMVpuro-ROR1-ΔPm) using FuGENE6 (Promega), followed by puromycin selection (1.0 μg ml^{-1}). The resultant stable clones were then seeded at $1x10^5$ cells per well in 6-well plates for immunofluorescence analysis and at $1x10^6$ cells in 10 cm dishes for IP-WB analysis, introduced with siControl or siROR1 on the next day, and harvested 2 days after siRNA transfection.

Immunofluorescence microscopy

A total of $5.0x10^4$ of NCI-H1975 or HeLa cells were plated onto coverslips in 12-well plates 24 hours before DNA and siRNA transfection. The cells were fixed with PBS containing 3.7% paraformaldehyde (PFA) at room temperature for 15 min. The fixed cells were permeabilized with PBS containing 0.1% Triton X-100. Non-specific binding was blocked by incubating the coverslips for 60 min in PBS-T (PBS with 0.1% Tween 20) containing 1.0% BSA (Roche). The fixed cells were incubated with primary antibodies (anti-HRS (1/500), anti-STAM1 (1/100), anti-RAB5 (1/500), anti-RAB7 (1/500), anti-EEA1 (1/500), anti-LAMP1 (1/500) or anti-CD63

(1/100) antibodies) diluted in PBS-T containing 1.0% BSA for overnight. Primary antibodies were washed with PBS-T three times and then incubated with the appropriate secondary antibodies conjugated to the specified Alexa dyes (Invitrogen) for 2 hours before mounting with SlowFade mounting solution (Invitrogen). Fluorescence was performed using Leica SP8 confocal laser microscope. For line scan analysis shown in Fig 3c, the fluorescent intensity of ROR1-GFP and mCherry-Rab5 were measured and plotted using ImageJ (Fiji) software. Diameter of $Rab5^{Q79L}$ compartment shown in Fig 7b was measured by ImageJ (Fiji) software and Quantification analysis (Welch's t-test) was performed by R software.

Super-resolution structured illumination microscopy (SIM)

mCherry-$Rab5^{Q79L}$- and ROR1-GFP-transfected HeLa cells were grown on cover slips (High-performance ISO8255 compliant/No. 1.5H, 170±5 μm, 18 mm x 18 mm [Carl Zeiss]) and fixed with 3.7% paraformaldehyde in PBS and then permeabilized with PBS containing 0.1% Triton X-100. The fixed cells were mounted with Vectashield H-1000 (Vector Laboratories, CA). Images were acquired with a Zeiss LSM 880 confocal microscope using an α Plan-Apochromat 100x/numerical aperture (N.A.) 1.46 objective. SIM images were collected on samples obtained with the Zeiss ELYRA PS.1 system (Carl Zeiss Microscopy) using a 100x objective lens with a numerical aperture of 1.46 at room temperature. Three orientation angles and five phases of the excitation grid were acquired for each Z plane, with Z spacing of 167.2 nm between planes. SIM processing was performed with SIM module of the ZEN 2 software (Carl Zeiss Microscopy).

Proximity Ligation Assay (PLA)

A total of $5.0x10^4$ of HeLa cells were plated onto coverslips in 12-well plates 24 hours before DNA transfection. Cells were fixed with 3.7% PFA in PBS for 15 min at room temperature,

permeabilized with 0.1% Triton X-100 in PBS for 15 min at room temperature, and blocked with Duolink blocking solution for 1 hr at 37°C. Incubation with primary antibodies (GFP and HRS, both at a 1:100 dilution in Duolink antibody diluent solution) were performed overnight at 4°C in a humidity chamber. The cells were washed twice for 10 min with Wash Buffer A, then incubated with PLUS and MINUS PLA probes solution for 1 hr at 37°C in a humidity chamber. The coverslips were washed again in Wash Buffer A, and then incubated in the Duolink Ligation Mix for 30 min at 37°C. The incubation was followed by washes with Wash Buffer A, the coverslips were incubated with the Duolink Amplification Mix for 100 min at 37°C and washed twice for 10 min each time with Wash Buffer B. Subsequently, the coverslips were sealed with SlowFade mounting solution with DAPI. Cells were imaged using a Leica SP8 laser confocal microscope and analyzed using LAS X software (Leica) and Image J based FIJI software.

Split-APEX2 Proximity biotin labelling

A total of $1.0x10^6$ of HeLa cells were plated in 10 cm dishes 24 hours before DNA transfection. Cells were co-transfected with the 5 ug of ROR1-AP_pLX304 and 5 ug of HRS-EX_pLX304 or STAM1-EX_pLX304 vectors using FuGENE HD reagent (Promega). 24 hr after transfection, Hemin was added (final concentration 5 uM) to culture medium and incubated for 90 min. After incubation, the cell culture medium was changed to DMEM with 500 uM biotin-phenol and incubated for 30 min at 37°C. Then H_2O_2 solution was added (final concentration 1 mM) and incubated for 1 min to initiate Proximity biotin labelling. To stop this labelling reaction, the cells were washed three times with a quencher solution (10 mM sodium azide, 10 mM sodium ascorbate, and 5 mM Trolox in PBS). Subsequently, the cells were lysed with RIPA buffer (50 mM Tris, 150 mM NaCl, 0.1% SDS, 0.5% sodium deoxycholate, 1.0% NP40) containing 10 mM sodium azide, 10 mM sodium ascorbate, 5 mM Trolox, and protease inhibitor cocktail

(Roche) on ice. The lysates were incubated for 10 min at 4°C and clarified by centrifugation at 13,000 rpm for 10 minutes at 4°C. The lysates were mixed with equilibrated NeutrAvidin coated magnetic beads for overnight at 4°C with gentle rotation. NeutrAvidin beads were then washed twice with RIPA buffer, once with 1M KCl, once with 0.1 M Na_2CO_3, once with 2M urea in 10 mM Tris-HCl, pH 8.0, and twice with RIPA buffer. Biotinylated proteins were eluted by incubating the beads with 1x SDS Sample Buffer (2% SDS, 10% Glycerol, 0.005%BPB, 62.5 mM Tris) supplemented with 5% 2-mercaptoethanol and 2 mM biotin and heating to 95 °C for 10 min. Biotinylated proteins were separated on a SuperSep Ace 12.5% gel (#199-14971, Wako Pure Chemical, Osaka, Japan) run for about 10 min at 20 mA. The gel was stained with SimplyBlue SafeStain (#LC6060, Thermo Fisher) and subsequently destained with water.

Mass Spectrometry

Biotinylated proteins were separated on a SuperSep Ace 12.5% gel (#199-14971, Wako Pure Chemical, Osaka, Japan) run for about 10 min at 20 mA. The gel was stained with SimplyBlue SafeStain (#LC6060, Thermo Fisher) and subsequently destained with water for in-gel digestion. The gel containing proteins was excised, cut into approximately 1mm sized pieces. Proteins in the gel pieces were reduced with DTT (#20291, Pierce/Thermo Fisher), alkylated with iodoacetamide (A39271, Pierce/Thermo Fisher), and digested with Trypsin/Lys-C Mix (V5073, Promega) in a buffer containing 40-mM ammonium bicarbonate (018-21742, Wako), pH 8.0, overnight at 37°C. The resultant peptides were analyzed on an Advance UHPLC system (AMR/Michrom Bioscience) coupled to a Q Exactive mass spectrometer (Thermo Fisher) processing the raw mass spectrum using Xcalibur (Thermo Fisher Scientific). The raw LC-MS/MS data was analyzed against the UniProtKB *Homo sapiens* database using Proteome Discoverer version 1.4 (Thermo Fisher) with the Mascot search engine version 2.5 or 2.6 (Matrix Science). A decoy database comprised of either randomized or reversed sequences in

the target database was used for false discovery rate (FDR) estimation, and Percolator algorithm was used to evaluate false positives. Search results were filtered against 1% global FDR for high confidence level. The resulting datasets were further analyzed with Scaffold 4 (Matrix Science/Proteome Software Inc.).

Electron microscopy

The siControl-, siROR1-, siHRS-, siSTAM1-treated NCI-H1975 cells were fixed with 2% paraformaldehyde (PFA) and 2% glutaraldehyde (GA) in 0.1 M phosphate buffer (PB) pH 7.4 at incubation temperature and then they were put into a refrigerator for 30 min in order to lower the temperature at 4˚C. Thereafter, they were fixed with 2 % GA in 0.1 M PB at 4˚C overnight. After these fixations the samples were washed 3 times with 0.1 M PB for 30 min each, and were postfixed with 2% osmium tetroxide (OsO_4) in 0.1 M PB at 4˚C for 1 hour. The samples were dehydrated in graded ethanol solutions (50%, 70%, 90%, and 100%). The schedule was as follows: 50% and 70% for 5 min each at 4˚C, 90% for 5 min at room temperature, and 3 changes of 100% for 5 min each at room temperature. The samples were transferred to a resin (Quetol-812; Nisshin EM Co., Tokyo, Japan), and were polymerized at 60˚C for 48 hours. The polymerized resins were ultra-thin sectioned at 70 nm with a diamond knife using an ultramicrotome (Ultracut UCT; Leica, Vienna, Austria) and the sections were mounted on copper grids. They were stained with 2% uranyl acetate at room temperature for 15 min, and then they were washed with distilled water followed by being secondary-stained with Lead stain solution (Sigma-Aldrich Co., Tokyo, Japan) at room temperature for 3 min. The grids were observed by a transmission electron microscopy (JEM-1400Plus; JEOL Ltd., Tokyo, Japan) at an acceleration voltage of 100kV. Digital images were taken with a CCD camera.

For determining the ROR1-GFP localization in $Rab5^{Q79L}$-induced MVEs or CD63-GFP localization in MVEs, the cells on the gold disks were frozen in liquid propane at -175˚C. Once

the samples were frozen, they were freeze substituted with 2% tannic acid in ethanol and 2% distilled water at -80˚C for 24 hours. Afterwards they were transferred where they can keep -20˚C for 4 hours, then they were warmed up to 4˚C for 1 hour. The samples were dehydrated, infiltrated, and then transferred to a fresh 100% resin, and were polymerized at 50˚C overnight. The polymerized resins were ultra-thin sectioned at 90 nm with a diamond knife using an ultramicrotome and the sections were placed on nickel grids. The grids were incubated with the primary antibody (rabbit anti-GFP pAb) in 1% BSA, PBS at 4˚C overnight, then they were washed with 1% BSA, PBS 3 times for 1 min. They were subsequently incubated with the secondary antibody conjugated to 10 nm gold particles (goat anti-rabbit IgG pAb) for 2 hours at room temperature. And after washing with PBS, the grids were placed in 2% glutaraldehyde in 0.1 M cacodylate buffer. Afterwards, the grids were dried and then were stained with 2% uranyl acetate for 15 min, and in Lead stain solution at room temperature for 3 min. The grids were observed by a transmission electron microscopy.

To define ROR1-APEX2 localization, HeLa cells expressing ROR1-APEX were fixed for 1 h with 2.5% glutaraldehyde in 0.1 mM sodium cacodylate buffer (CB; pH 7.4) containing 1 mM $CaCl_2$. After rinses, the samples were incubated for 5–15 min in 1.0 mg/mL DAB and 0.03% H_2O_2 in CB and post-fixed for 1 h with 2% osmium tetroxide in CB. They were stained for 2 h with 2% uranyl acetate in distilled water, dehydrated in a grade series of ethanol, and embedded in epoxy resin. Ultrathin sections counterstained with lead citrate were observed under a JEM1011 electron microscope.

Preparation of recombinant proteins

GST-tagged ROR1 (intracellular domain) was expressed in Sf9 insect cells using a Gateway system (Invitrogen) according to the manufacturer's instructions. Recombinant GST-tagged ROR1-WT protein was purified by glutathione-affinity chromatography. GST was purchased

from Abnova (Taipei). Purification was performed according to the manufacturer's instructions, and the purified proteins were stored at -80°C for GST-pull down assay.

GST pull-down assay

The NCI-H1975 cells were solubilized in octylglucoside buffer (60 mM octylglucoside, 150 mM NaCl and 50 mM EDTA). The cell extracts were mixed with glutathione beads coated with recombinant GST-tagged ROR1. After several rounds of washing, the bound proteins were eluted and subjected to SDS-PAGE followed by WB analysis using anti-GST, anti-HRS or anti-STAM1 antibodies.

Rab5 activation assay

For Rab5 GTPase activation assay, the cells were treated with siROR1, and amount of GTP-form Rab5 was measured 48 h later with a Rab5 activation assay kit (NewEast Biosciences, Malvern, PA) according to the manufacturer's instructions. Briefly, the cells were washed twice with ice-cold PBS and lysed in an ice-cold 1× assay/lysis buffer for 20 min on ice. The lysates were transferred to appropriately sized tubes and cleared at 12,000 *g* for 10 min at 4°C. The supernatants were then collected to a microcentrifuge tube, and anti-active Rab5 MAb (1:1,000) and 20 μl of resuspended bead slurry were added. The tubes were incubated at 4°C for 1 h with gentle agitation, followed by aspiration and discarding of the supernatant by centrifugation for 1 min at 5,000 *g*. We then resuspended the bead pellet in reducing SDS-PAGE sample buffer, boiled it for 5 min, and then processed it for SDS-PAGE and immunoblotting detection.

EVs purification from conditioned media

For conditioned media, the cells seeded in T300 flask. Next day, the cells were washed with phosphate-buffered saline (PBS), and the culture medium was replaced with advanced RPMI

1640 medium for NCI-H1975, H23 and PC9 cells. For HPL1D, the EVs producing culture was started with HPL1D complete medium without FBS. After incubation for 48 h, the culture supernatant was collected and centrifuged at 2,000 g for 10 min at 4˚C. To thoroughly remove cellular debris, the supernatant was filtered through a 0.22 mm filter (#SLGVR33RS, Millipore). The filtrated culture supernatant was then used for EV isolation. To prepare EVs, culture supernatant was ultracentrifuged at 110,000 g for 70 min at 4˚C. The pellets were washed with 35 ml of PBS, ultracentrifuged at 110,000 g for 70 min at 4˚C and resuspended in PBS. RNA inference was using reverse transfection protocol and collect culture medium after 48hr.

Particle size and concentration by NTA

Nanoparticle tracking analysis (NTA) was carried out using the Nanosight system on purified EVs diluted 4-fold with PBS for analysis. A 60s video recorded all events for further analysis by NTA software.

ACKNOWLEDGMENTS

We thank Y. Ikeda, Y. Watanabe and J. Hirai for their technical support. We are also grateful for the expert assistance from S. Kawamura for electron microscopy analysis. This work was supported by MEXT KAKENHI, Grant-in-Aid for Science Research (B) Grant Number JP18959589 and Grant-in-Aid for Challenging Research (Exploratory) Grant Number JP19095157; MEXT Leading Initiative for Excellent Young Researchers Grant Number JP16811388; JST, PRESTO Grant Number JP17937947, Japan.

AUTHOR CONTRIBUTIONS

T.Y. conceived and designed the research. T.Y., M.Yamamoto., M.Yamazaki., M.S., H.D., and H.L. performed the biochemical experiments. T.Y., M.Yamamoto., and M.Yamazaki. performed the cell experiments. T.Y., M.Yamamoto., and M.Yamazaki. performed the molecular biological experiments. T.Y. and M.Yamamoto. performed the immunofluorescence microscopy. T.F. performed the electron microscopy. N.T. performed the mass spectrometry analysis. T.Y., M.Yamamoto., M.Yamazaki., C.O., T.F., and T.T. wrote the manuscript.

COMPETING FINANCIAL INTERESTS

The authors declare no competing financial interests.

REFERENCES

1. Huotari J, Helenius A. Endosome maturation. *EMBO J* **30**, 3481-3500 (2011).

2. Scott CC, Vacca F, Gruenberg J. Endosome maturation, transport and functions. *Semin Cell Dev Biol* **31**, 2-10 (2014).

3. Wandinger-Ness A, Zerial M. Rab proteins and the compartmentalization of the endosomal system. *Cold Spring Harb Perspect Biol* **6**, a022616 (2014).

4. Gruenberg J, Stenmark H. The biogenesis of multivesicular endosomes. *Nat Rev Mol Cell Biol* **5**, 317-323 (2004).

5. Hanson PI, Cashikar A. Multivesicular body morphogenesis. *Annu Rev Cell Dev Biol* **28**, 337-362 (2012).

6. Katzmann DJ, Odorizzi G, Emr SD. Receptor downregulation and multivesicular-body sorting. *Nat Rev Mol Cell Biol* **3**, 893-905 (2002).

7. Piper RC, Katzmann DJ. Biogenesis and function of multivesicular bodies. *Annu Rev Cell Dev Biol* **23**, 519-547 (2007).

8. Colombo M, Raposo G, Thery C. Biogenesis, secretion, and intercellular interactions of exosomes and other extracellular vesicles. *Annu Rev Cell Dev Biol* **30**, 255-289 (2014).

9. Kowal J, Tkach M, Thery C. Biogenesis and secretion of exosomes. *Curr Opin Cell Biol* **29**, 116-125 (2014).

10. Simons M, Raposo G. Exosomes--vesicular carriers for intercellular communication. *Curr Opin Cell Biol* **21**, 575-581 (2009).

11. van Niel G, Porto-Carreiro I, Simoes S, Raposo G. Exosomes: a common pathway for a specialized function. *J Biochem* **140**, 13-21 (2006).

12. Williams RL, Urbe S. The emerging shape of the ESCRT machinery. *Nat Rev Mol Cell Biol* **8**, 355-368 (2007).

13. Hurley JH, Hanson PI. Membrane budding and scission by the ESCRT machinery: it's

all in the neck. *Nat Rev Mol Cell Biol* **11**, 556-566 (2010).

14. McCullough J, Colf LA, Sundquist WI. Membrane fission reactions of the mammalian ESCRT pathway. *Annu Rev Biochem* **82**, 663-692 (2013).

15. Gatta AT, Carlton JG. The ESCRT-machinery: closing holes and expanding roles. *Curr Opin Cell Biol* **59**, 121-132 (2019).

16. Geminard C, De Gassart A, Blanc L, Vidal M. Degradation of AP2 during reticulocyte maturation enhances binding of hsc70 and Alix to a common site on TFR for sorting into exosomes. *Traffic* **5**, 181-193 (2004).

17. Baietti MF*, et al.* Syndecan-syntenin-ALIX regulates the biogenesis of exosomes. *Nat Cell Biol* **14**, 677-685 (2012).

18. Hoshino D*, et al.* Exosome secretion is enhanced by invadopodia and drives invasive behavior. *Cell Rep* **5**, 1159-1168 (2013).

19. Gross JC, Chaudhary V, Bartscherer K, Boutros M. Active Wnt proteins are secreted on exosomes. *Nat Cell Biol* **14**, 1036-1045 (2012).

20. Tamai K*, et al.* Exosome secretion of dendritic cells is regulated by Hrs, an ESCRT-0 protein. *Biochem Biophys Res Commun* **399**, 384-390 (2010).

21. Colombo M*, et al.* Analysis of ESCRT functions in exosome biogenesis, composition and secretion highlights the heterogeneity of extracellular vesicles. *J Cell Sci* **126**, 5553-5565 (2013).

22. Yamaguchi T*, et al.* NKX2-1/TITF1/TTF-1-Induced ROR1 is required to sustain EGFR survival signaling in lung adenocarcinoma. *Cancer Cell* **21**, 348-361 (2012).

23. Yamaguchi T, Hosono Y, Yanagisawa K, Takahashi T. NKX2-1/TTF-1: an enigmatic oncogene that functions as a double-edged sword for cancer cell survival and progression. *Cancer Cell* **23**, 718-723 (2013).

24. Yamaguchi T*, et al.* ROR1 sustains caveolae and survival signalling as a scaffold of cavin-1 and caveolin-1. *Nat Commun* **7**, 10060 (2016).

25. Yamaguchi T*, et al.* ROR1-CAVIN3 interaction required for caveolae-dependent

endocytosis and pro-survival signaling in lung adenocarcinoma. *Oncogene* **38**, 5142-5157 (2019).

26. Bache KG, Brech A, Mehlum A, Stenmark H. Hrs regulates multivesicular body formation via ESCRT recruitment to endosomes. *J Cell Biol* **162**, 435-442 (2003).

27. Razi M, Futter CE. Distinct roles for Tsg101 and Hrs in multivesicular body formation and inward vesiculation. *Mol Biol Cell* **17**, 3469-3483 (2006).

28. Liu L, Pilch PF. A critical role of cavin (polymerase I and transcript release factor) in caveolae formation and organization. *J Biol Chem* **283**, 4314-4322 (2008).

29. Stenmark H, Parton RG, Steele-Mortimer O, Lutcke A, Gruenberg J, Zerial M. Inhibition of rab5 GTPase activity stimulates membrane fusion in endocytosis. *EMBO J* **13**, 1287-1296 (1994).

30. Schermelleh L, Heintzmann R, Leonhardt H. A guide to super-resolution fluorescence microscopy. *J Cell Biol* **190**, 165-175 (2010).

31. Lam SS*, et al.* Directed evolution of APEX2 for electron microscopy and proximity labeling. *Nat Methods* **12**, 51-54 (2015).

32. Hung V*, et al.* Proteomic mapping of the human mitochondrial intermembrane space in live cells via ratiometric APEX tagging. *Mol Cell* **55**, 332-341 (2014).

33. Rhee HW*, et al.* Proteomic mapping of mitochondria in living cells via spatially restricted enzymatic tagging. *Science* **339**, 1328-1331 (2013).

34. Asao H*, et al.* Hrs is associated with STAM, a signal-transducing adaptor molecule. Its suppressive effect on cytokine-induced cell growth. *J Biol Chem* **272**, 32785-32791 (1997).

35. Prag G*, et al.* The Vps27/Hse1 complex is a GAT domain-based scaffold for ubiquitin-dependent sorting. *Dev Cell* **12**, 973-986 (2007).

36. Henne WM, Buchkovich NJ, Emr SD. The ESCRT pathway. *Dev Cell* **21**, 77-91 (2011).

37. Han Y*, et al.* Directed Evolution of Split APEX2 Peroxidase. *ACS Chem Biol* **14**, 619-

635 (2019).

38. Lievens S, Tavernier J. Single protein complex visualization: seeing is believing. *Nat Methods* **3**, 971-972 (2006).

39. Soderberg O*, et al.* Direct observation of individual endogenous protein complexes in situ by proximity ligation. *Nat Methods* **3**, 995-1000 (2006).

40. Wegner CS*, et al.* Ultrastructural characterization of giant endosomes induced by GTPase-deficient Rab5. *Histochem Cell Biol* **133**, 41-55 (2010).

41. Hojjat-Farsangi M*, et al.* The receptor tyrosine kinase ROR1--an oncofetal antigen for targeted cancer therapy. *Semin Cancer Biol* **29**, 21-31 (2014).

42. Fukuda T*, et al.* Antisera induced by infusions of autologous Ad-CD154-leukemia B cells identify ROR1 as an oncofetal antigen and receptor for Wnt5a. *Proc Natl Acad Sci U S A* **105**, 3047-3052 (2008).

43. Niendorf S*, et al.* Essential role of ubiquitin-specific protease 8 for receptor tyrosine kinase stability and endocytic trafficking in vivo. *Mol Cell Biol* **27**, 5029-5039 (2007).

44. Lloyd TE, Atkinson R, Wu MN, Zhou Y, Pennetta G, Bellen HJ. Hrs regulates endosome membrane invagination and tyrosine kinase receptor signaling in Drosophila. *Cell* **108**, 261-269 (2002).

45. de Gassart A, Geminard C, Fevrier B, Raposo G, Vidal M. Lipid raft-associated protein sorting in exosomes. *Blood* **102**, 4336-4344 (2003).

46. Toyoshima M*, et al.* Inhibition of tumor growth and metastasis by depletion of vesicular sorting protein Hrs: its regulatory role on E-cadherin and beta-catenin. *Cancer Res* **67**, 5162-5171 (2007).

47. da Rocha AA*, et al.* Hepatocyte growth factor-regulated tyrosine kinase substrate (HGS) and guanylate kinase 1 (GUK1) are differentially expressed in GH-secreting adenomas. *Pituitary* **9**, 83-92 (2006).

48. Lustig B, Behrens J. The Wnt signaling pathway and its role in tumor development. *J Cancer Res Clin Oncol* **129**, 199-221 (2003).

49. Komada M, Soriano P. Hrs, a FYVE finger protein localized to early endosomes, is implicated in vesicular traffic and required for ventral folding morphogenesis. *Genes Dev* **13**, 1475-1485 (1999).

50. Kanazawa C*, et al.* Effects of deficiencies of STAMs and Hrs, mammalian class E Vps proteins, on receptor downregulation. *Biochem Biophys Res Commun* **309**, 848-856 (2003).

51. Zhang S*, et al.* ROR1 is expressed in human breast cancer and associated with enhanced tumor-cell growth. *PLoS One* **7**, e31127 (2012).

52. Zhang S*, et al.* The onco-embryonic antigen ROR1 is expressed by a variety of human cancers. *Am J Pathol* **181**, 1903-1910 (2012).

53. Gentile A, Lazzari L, Benvenuti S, Trusolino L, Comoglio PM. Ror1 is a pseudokinase that is crucial for Met-driven tumorigenesis. *Cancer Res* **71**, 3132-3141 (2011).

54. Zhang S*, et al.* Ovarian cancer stem cells express ROR1, which can be targeted for anti-cancer-stem-cell therapy. *Proc Natl Acad Sci U S A* **111**, 17266-17271 (2014).

55. Bicocca VT*, et al.* Crosstalk between ROR1 and the Pre-B cell receptor promotes survival of t(1;19) acute lymphoblastic leukemia. *Cancer Cell* **22**, 656-667 (2012).

56. Daneshmanesh AH*, et al.* Ror1, a cell surface receptor tyrosine kinase is expressed in chronic lymphocytic leukemia and may serve as a putative target for therapy. *Int J Cancer* **123**, 1190-1195 (2008).

57. Baskar S*, et al.* Unique cell surface expression of receptor tyrosine kinase ROR1 in human B-cell chronic lymphocytic leukemia. *Clin Cancer Res* **14**, 396-404 (2008).

Figure legends

Figure 1 | ROR1 knockdown results in decreased HRS and STAM1 protein expression.

(**a**) Representative electron microscopy findings. ROR1 knockdown resulted in typically large and ring-shaped vacuoles containing few internal vesicles in NCI-H1975 lung cancer cells. In contrast, siControl-treated cells showed an intact multivesicular endosome (MVE). Scale bar, 200nm. See Supplementary Fig 1, which shows similar effects in siHRS- and siSTAM1-treated cells. (**b**) HRS and STAM1, but not TGN38 or GM130, were decreased with use of ROR1 siRNA. (**c**) WB analysis revealed decreased expressions of HRS and STAM1 in NCI-H1975, PC-9, and SK-LC-5 cell lines treated with siROR1. (**d**) WB analysis revealed decreased levels and easily detectable retention of HRS and STAM1 expressions in NCI-H1975 cells at 24 hours after siROR1 transfection. (**e**) Immunofluorescence staining showed markedly altered localization of Rab7 and CD63 following ROR1 knockdown. Scale bar, 30 μm. (**f**) Quantification of CD63 localization. Data from (**e**) are presented as percentages of intracellular CD63 signal-positive cells (Dispersal or Accumulation). Values reflect the mean ± SD of two independent experiments, with an average of 20 cells scored per experiment.

Figure 2 | ROR1 interacts with HRS and STAM1.

(**a**) IP-WB analysis using octylglucoside as a detergent showed an association of ROR1 with HRS and STAM1 in PC-9 and NCI-H1975 cells. (**b**) An interaction of ROR1 with HRS and STAM1 was shown by IP-WB analysis of A549 cells transfected with ROR1-GFP. (**c**) Pull-down assay results using purified ROR1 protein showed physical associations of ROR1 with HRS and STAM1. (**d**) ROR1-GFP along with endogenous HRS or STAM1 colocalization in HeLa cells was shown by immunofluorescence analysis. Scale bar, 30 μm.

Figure 3 | ROR1 localized in Rab5-induced MVEs.

(**a**) Colocalization of mCherry-Rab5^{Q79L}, ROR1-GFP, HRS, and CD63 shown by immunofluorescence analysis results. Also see Supplementary Fig 2, which presents findings showing colocalization of mCherry-Rab5^{Q79L}, ROR1-GFP, HRS, and EEA1. Scale bar, 30 μm. (**b**) Localization of ROR1 in Rab5-induced MVEs in HeLa cells was shown by immunofluorescence analysis using super-resolution structured illumination microscopy. Localization of ROR1-GFP is indicated with arrowheads. Scale bar, 5 μm. (**c**) Confocal images indicating colocalization of ROR1 with Rab5 in Rab5^{Q79L}-expressed cells. Areas of colocalization are shown by line intensity profiles. (**d**) Electron microscopy was used to analyze HeLa cells expressing ROR1-GFP after immunogold labeling of cryosections using antibodies against GFP. ROR1-GFP is indicated with arrowheads. Localization of ROR1-GFP was noted in both the limiting membranes and intraluminal vesicles (ILVs) of Rab5-induced MVEs. Scale bar, 200 nm. (**e**) Representative electron microscopy images of HeLa cells transfected with ROR1-APEX2. The results showed ROR1-APEX2 present in both the limiting membranes and ILVs of MVEs. Arrowheads indicate ROR1-APEX2-positive structures. Scale bar, 200 nm. Also see Supplementary Fig 3a and 3b showing confirmation of biotin labeling of ROR1-APEX2 by immunofluorescence and WB analysis.

Figure 4 | ROR1 required for prevention of HRS routing to lysosomes.

(**a**) IP-WB analysis demonstrated an impaired association between HRS and STAM1 in siROR1-treated PC-9 and NCI-H1975 cells. Cell lysates were harvested 24 hours after siROR1 transfection, when no obvious siROR1-induced reduction of HRS and STAM1 expression was seen. (**b**) Immunofluorescence analysis showed significant colocalization of HRS with LAMP-1 at 24 hours after siROR1 treatment. Scale bar, 30 μm.

Figure 5 | ROR1-STAM1 interaction required for HRS-STAM1 binding.

(**a**) IP-WB analysis showing impaired association of ROR1 with HRS, but not CAVIN1, in NCI-H1975 cells following STAM1 knockdown. Cell lysates were harvested at 24 hours after siSTAM1 transfection, when no obvious siSTAM1-induced reduction of HRS expression was seen. (**b**) Immunofluorescence analysis showing markedly impaired colocalization of ROR1 and HRS induced by STAM1 knockdown. Scale bar, 30 μm. (**c**) The proline-rich domain of ROR1 was demonstrated as the STAM1-binding region in IP-WB analysis with various ROR1 deletion mutants. (**d**) IP-WB analysis showed an impaired association of HRS with STAM1 in ROR1-ΔPm-reconstituted NCI-H1975 cells. TF, transfectant (**e**) Immunofluorescence analysis indicated significant colocalization of HRS with LAMP-1 in ROR1-ΔPm-reconstituted NCI-H1975 cells. Scale bar, 30 μm.

Figure 6 | Identification of Rab5 as ROR1-HRS binding protein.

(**a**) Schematic overview of split-APEX2. Two inactive fragments have an ability to reconstitute resulting in active peroxidase when driven together by ROR1-HRS interaction. See Supplementary Fig 4a for a schematic overview regarding split-APEX2 testing of ROR1-STAM1. (**b**) Biotin labeling was examined using confocal imaging. HeLa cells were transfected with ROR1-AP and HRS-EX, then biotin labeling was initiated with H_2O_2 following biotin-phenol incubation. Scale bar, 30 μm. See Supplementary Fig 4b for findings regarding ROR1-STAM1. (**c**) WB analysis was used to test biotin labeling in live cells. Cells were treated as noted in (**b**). Whole cell lysates were resolved by SDS-PAGE and tested for biotinylated proteins using streptavidin-HRP. See Supplementary Fig 4c for findings regarding ROR1-STAM1. (**d**) Schematic diagram of strategy for use of split-APEX2 system and LC-MS/MS analysis. 70 proteins were identified only in ROR1-AP- and HRS-EX-transfected HeLa cells. See Supplementary Fig 4d for findings regarding ROR1-STAM1. (**e**) PLA assays were conducted using mouse anti-GFP and rabbit anti-HRS antibodies.

Arrowheads indicate purple foci representing ROR1 in close proximity with HRS in the limiting membrane of Rab5-induced MVEs. Images shown are three-dimensional reconstructions from a series of confocal Z-stack images. Scale bar, 30 μm.

Figure 7 | ROR1 required for formation of Rab5-induced MVEs.

(**a**) Effect of ROR1 deletion on $Rab5^{Q79L}$-induced MVE formation. HeLa cells were treated with siControl or siROR1, then transfected with mCherry-$Rab5^{Q79L}$. Cells were fixed and examined using confocal microscopy. Images shown are three-dimensional reconstructions from a series of confocal Z-stack images. Scale bar, 30 μm. (**b**) Quantification of diameters of $Rab5^{Q79L}$-induced MVEs. Findings shown in (**a**) indicating endosome diameter were determined using the line tool of the Image J software package. Lines represent the median, and boxes show the 25th and 75th percentiles of endosome diameters in siControl- and siROR1-treated cells. Whiskers indicate SD. A total of 158 endosomes (siControl) and 124 endosomes (siROR1) from each 11 cells were analyzed. Data were analyzed using Welch's two sample t-test (**$P<0.001$). (**c**) Confocal imaging of siROR1-treated HeLa cells showed $Rab5^{Q79L}$-induced MVEs to be very small, with those structures surrounded by LAMP-1-positive vesicles. Scale bar, 30 μm. (**d**) ROR1 knockdown reduced GTP-bound Rab5. NCI-H1975 cells were transfected with siControl or siROR1, then processed for total protein extraction followed by an Rab5 activity assay, as described in Methods. (**e**) IP-WB analysis showing association between ROR1 and GTP-bound Rab5 in $Rab5^{WT}$- and $Rab5^{Q79L}$-transfected NCI-H1975 cells.

Figure 8 | ROR1 depletion inhibited formation of CD63-positive MVEs and reduced exosome release.

(**a**) Representative results of immunoelectron microscopy. After immunogold labeling of

cryosections using antibodies against GFP, HeLa cells expressing CD63-GFP were analyzed by electron microscopy. CD63-GFP, indicated by arrowheads, was found localized in ILVs of MVEs in siControl-treated cells. In contrast, siROR1-treated cells showed only CD63-GFP in that area, possibly a vestige of MVE. Scale bar, 200 nm. (**b**) Purification of exosomes from conditioned media of cancer cell lines was performed by sequential centrifugation. Whole-cell lysates of NCI-H1975, PC-9, and NCI-H23 lung cancer cell lines, as well as HPL1D human peripheral lung epithelial cells were subjected to WB analysis with the indicated antibodies. The total exosome fraction isolated from conditioned media of the cell lines by sequential centrifugation was also subjected to WB analysis. (**c**) NCI-H1975 cells were transfected with siControl, siROR1, siHRS, or siSTAM1, then conditioned medium samples were subjected to exosome preparation, followed by an NTA assay for quantitative measurement of isolated exosome particles. Values reflect the mean ± SD of three independent experiments. (**d**) Schematic diagram of proposed model showing how ROR1 sustains MVE formation and exosome biogenesis. ROR1 facilitates the interaction of HRS with STAM1 at the limiting membrane of Rab5-induced endosomes, which results in sustained MVEs formation and exosome biogenesis via its scaffold function for HRS and STAM1 in human cancer cells.

Supplementary Figure 1 | Typical large and ring-shaped vacuoles containing few internal vesicles were observed in siROR1-, siHRS-, and siSTAM1-treated cells. Representative electron microscopy results. ROR1, HRS, or STAM1 knockdown in NCI-H1975 lung cancer cells resulted in typically large and ring-shaped vacuoles that contained few internal vesicles. In contrast, the cytoplasm of siControl-treated cells showed no abnormal vesicles. Asterisk (*) indicates lipid droplet, suggesting that chemical fixation had the anticipated effect. Note showing abnormal vesicle indicates that it was not caused by improper fixing. Scale bar, 200 nm.

Supplementary Figure 2 | Colocalization of ROR1 with HRS and EEA1 in Rab5^{Q79L}-induced endosomes.

Colocalization of mCherry-Rab5^{Q79L}, ROR1-GFP, HRS, and EEA1 shown by immunofluorescence analysis.

Supplementary Figure 3 | Confirmation of biotin labeling of ROR1-APEX2.

(**a**) Biotin labeling was examined using confocal imaging. HeLa cells were transfected with ROR1-APEX2, then biotin labeling was initiated with H_2O_2 following biotin-phenol incubation. Scale bar, 30 μm. (**b**) WB analysis was performed to test biotin labeling in live cells. Cells were treated as noted in (**a**). Whole cell lysates were resolved by SDS-PAGE and tested by streptavidin-HRP for biotinylated proteins.

Supplementary Figure 4 | Identification of Rab5 as ROR1-STAM1 binding protein.

(**a**) Schematic overview of split-APEX2. When driven by a ROR1-STAM1 interaction, inactive fragments are able to reconstitute to give active peroxidase. (**b**) Biotin labeling was examined using confocal imaging. HeLa cells were transfected with ROR1-AP and STAM1-EX, then biotin labeling was initiated with H_2O_2 following biotin-phenol incubation. Scale bar, 30 μm. (**c**) WB analysis was used to test biotin labeling in live cells. Cells were treated as noted in (**b**). Whole cell lysates were resolved by SDS-PAGE and examined by streptavidin-HRP for biotinylated proteins. (**d**) Schematic diagram of strategy using split-APEX2 system and LC-MS/MS analysis. 72 proteins were identified only in ROR1-AP- and STAM1-EX-transfected HeLa cells.

Supplementary Figure 5 | NTA assay for quantitative measurement of isolated exosome

particles.

Representative findings obtained in NTA assays are shown. The results demonstrated similar size distribution in isolated exosome particles from siControl-, siROR1-, siHRS-, and siSTAM1-treated NCI-H1975 lung cancer cells.

Figures

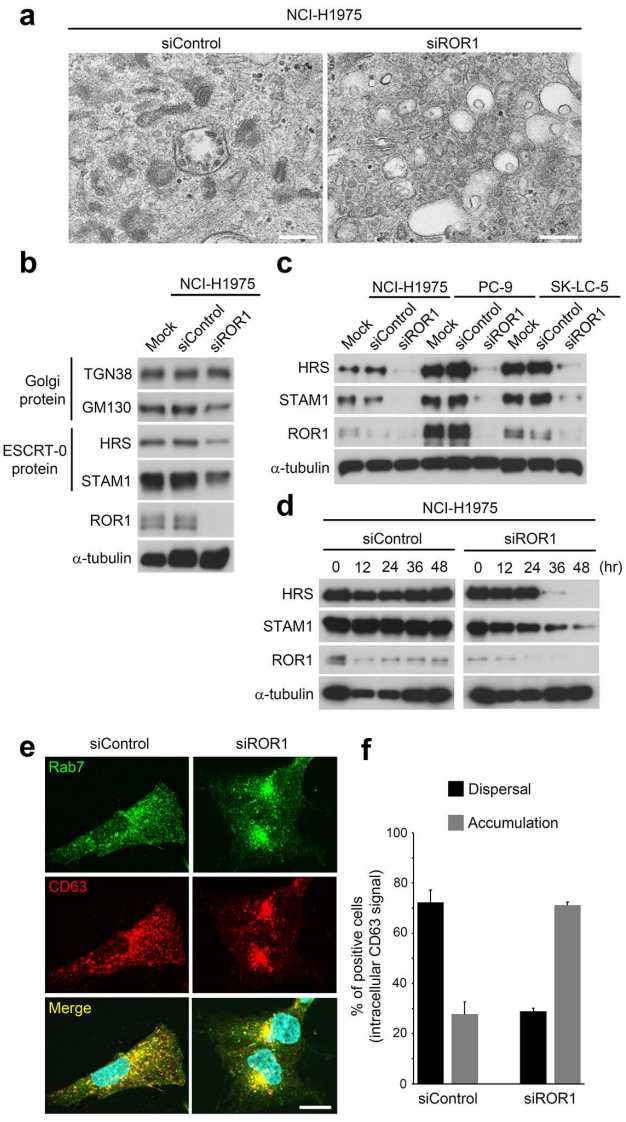

Figure 1

Figure 1

ROR1 knockdown results in decreased HRS and STAM1 protein expression. (a) Representative electron microscopy findings. ROR1 knockdown resulted in typically large and ring-shaped vacuoles containing few internal vesicles in NCI-H1975 lung cancer cells. In contrast, siControl-treated cells showed an intact

multivesicular endosome (MVE). Scale bar, 200nm. See Supplementary Fig 1, which shows similar effects in siHRS- and siSTAM1- treated cells. (b) HRS and STAM1, but not TGN38 or GM130, were decreased with use of ROR1 siRNA. (c) WB analysis revealed decreased expressions of HRS and STAM1 in NCIH1975, PC-9, and SK-LC-5 cell lines treated with siROR1. (d) WB analysis revealed decreased levels and easily detectable retention of HRS and STAM1 expressions in NCIH1975 cells at 24 hours after siROR1 transfection. (e) Immunofluorescence staining showed markedly altered localization of Rab7 and CD63 following ROR1 knockdown. Scale bar, 30 μm. (f) Quantification of CD63 localization. Data from (e) are presented as percentages of intracellular CD63 signal-positive cells (Dispersal or Accumulation). Values reflect the mean ± SD of two independent experiments, with an average of 20 cells scored per experiment.

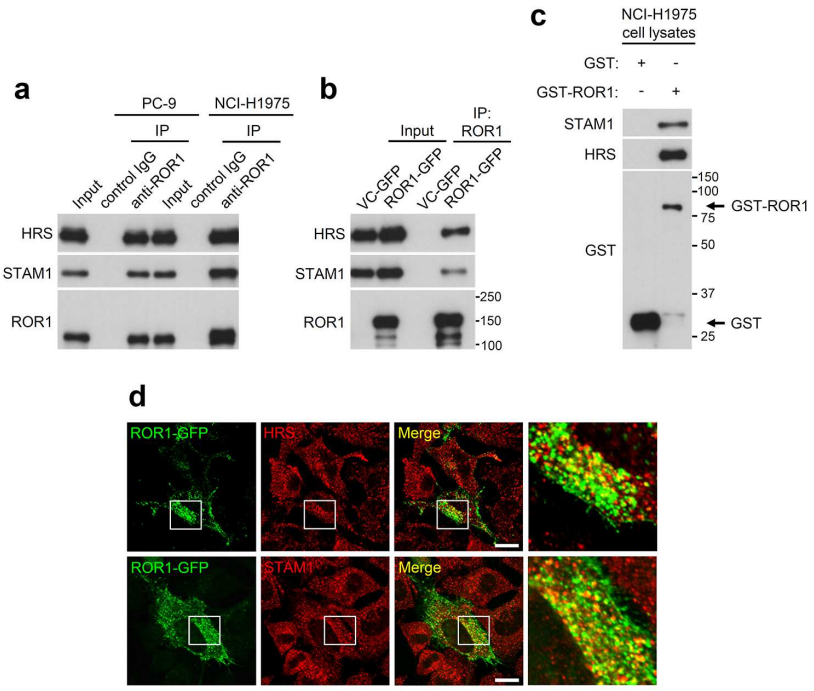

Figure 2

Figure 2

ROR1 interacts with HRS and STAM1. (a) IP-WB analysis using octylglucoside as a detergent showed an association of ROR1 with HRS and STAM1 in PC-9 and NCI-H1975 cells. (b) An interaction of ROR1 with HRS and STAM1 was shown by IP-WB analysis of A549 cells transfected with ROR1-GFP. (c) Pulldown assay results using purified ROR1 protein showed physical associations of ROR1 with HRS and STAM1.

(d) ROR1-GFP along with endogenous HRS or STAM1 colocalization in HeLa cells was shown by immunofluorescence analysis. Scale bar, 30 μm.

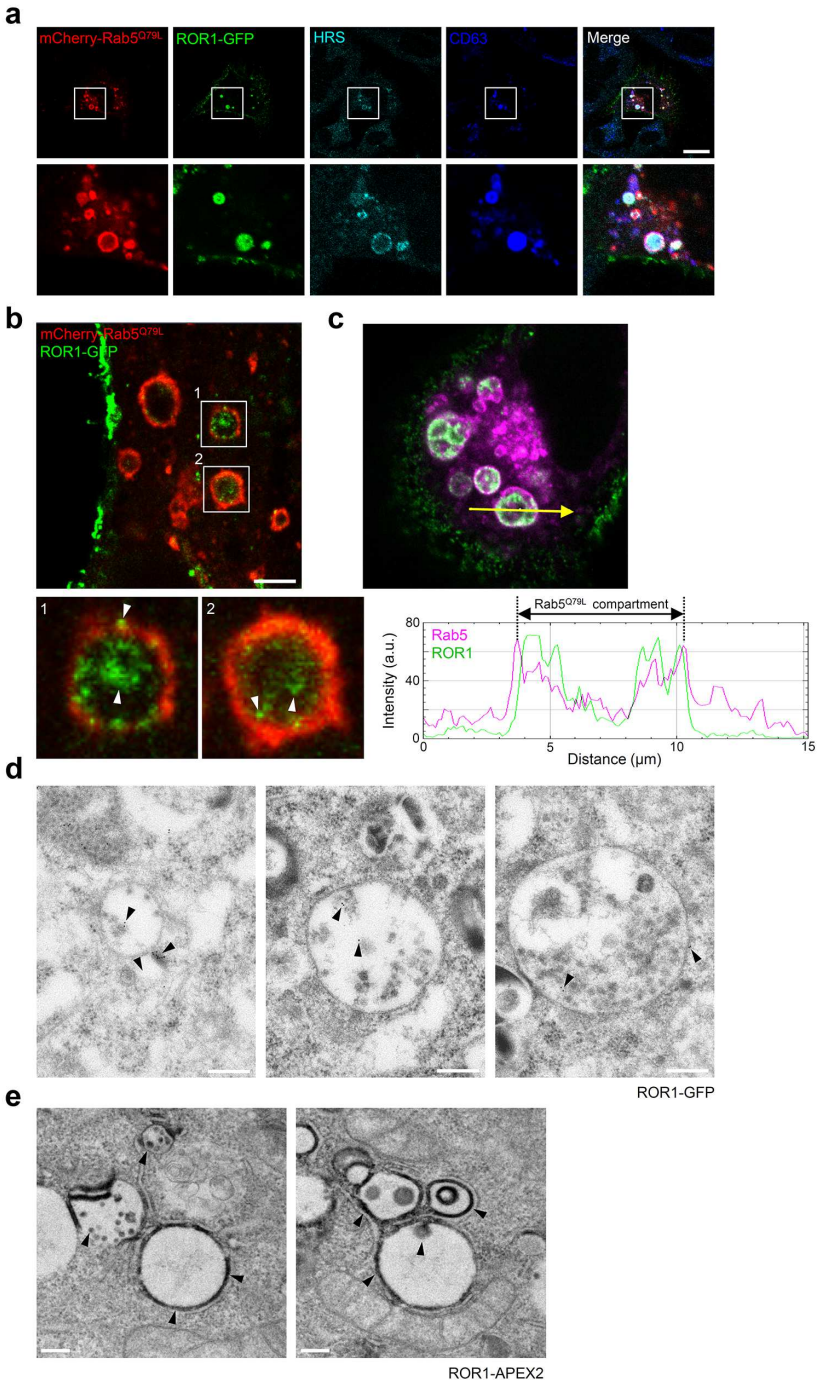

Figure 3

Figure 3

ROR1 localized in Rab5-induced MVEs. 35 (a) Colocalization of mCherry-Rab5Q79L, ROR1-GFP, HRS, and CD63 shown by immunofluorescence analysis results. Also see Supplementary Fig 2, which presents findings showing colocalization of mCherry-Rab5Q79L, ROR1-GFP, HRS, and EEA1. Scale bar, 30 μm. (b)

Localization of ROR1 in Rab5-induced MVEs in HeLa cells was shown by immunofluorescence analysis using super-resolution structured illumination microscopy. Localization of ROR1-GFP is indicated with arrowheads. Scale bar, 5 μm. (c) Confocal images indicating colocalization of ROR1 with Rab5 in Rab5Q79L-expressed cells. Areas of colocalization are shown by line intensity profiles. (d) Electron microscopy was used to analyze HeLa cells expressing ROR1-GFP after immunogold labeling of cryosections using antibodies against GFP. ROR1-GFP is indicated with arrowheads. Localization of ROR1-GFP was noted in both the limiting membranes and intraluminal vesicles (ILVs) of Rab5-induced MVEs. Scale bar, 200 nm. (e) Representative electron microscopy images of HeLa cells transfected with ROR1-APEX2. The results showed ROR1-APEX2 present in both the limiting membranes and ILVs of MVEs. Arrowheads indicate ROR1-APEX2-positive structures. Scale bar, 200 nm. Also see Supplementary Fig 3a and 3b showing confirmation of biotin labeling of ROR1-APEX2 by immunofluorescence and WB analysis.

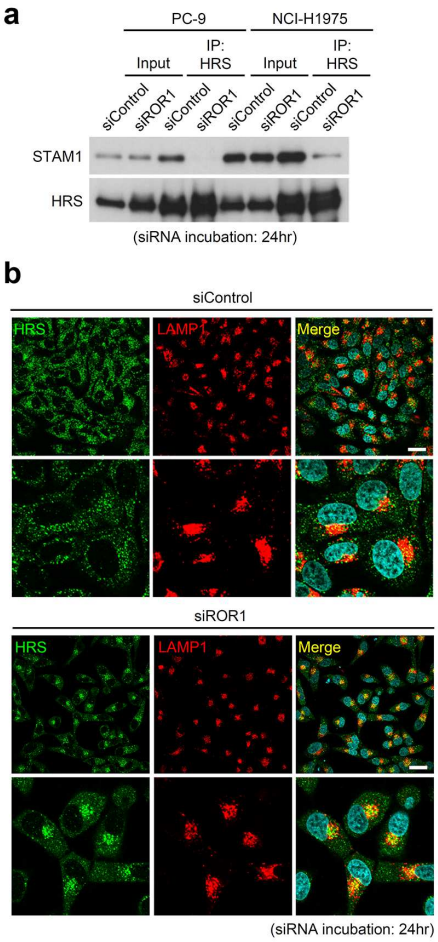

Figure 4

Figure 4

ROR1 required for prevention of HRS routing to lysosomes. (a) IP-WB analysis demonstrated an impaired association between HRS and STAM1 in siROR1-treated PC-9 and NCI-H1975 cells. Cell lysates were harvested 24 hours after siROR1 transfection, when no obvious siROR1-induced reduction of HRS and STAM1 expression was seen. (b) Immunofluorescence analysis showed significant colocalization of HRS with LAMP-1 at 24 hours after siROR1 treatment. Scale bar, 30 μm.

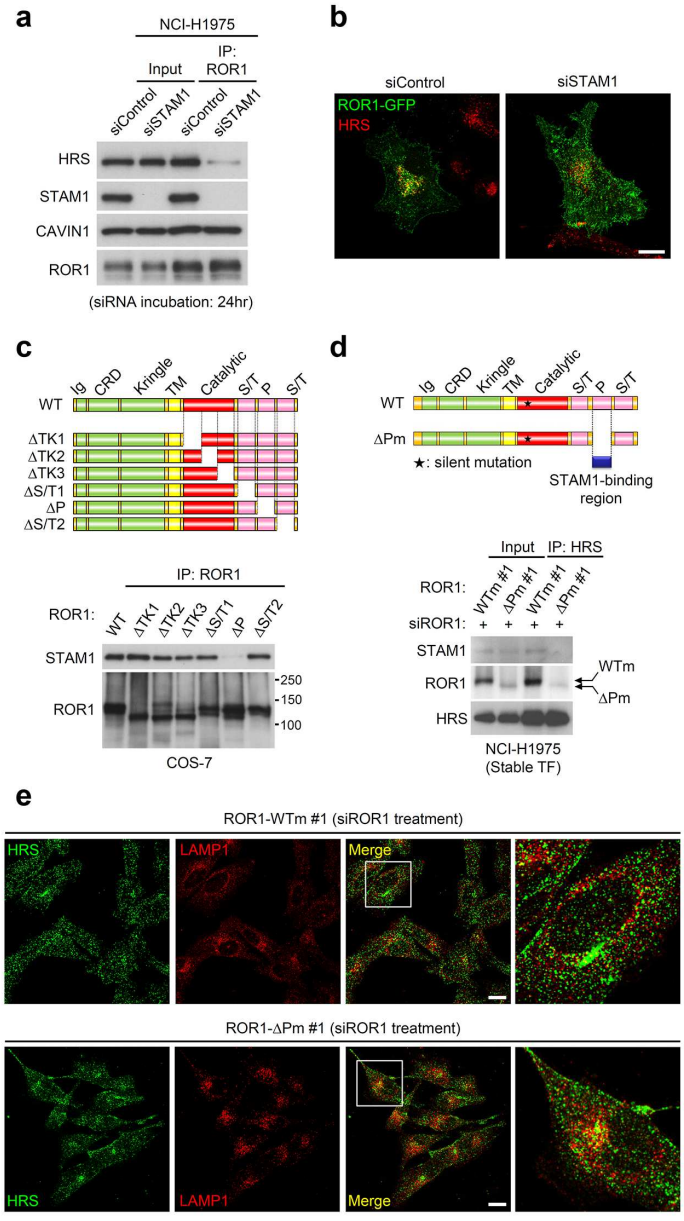

Figure 5

Figure 5

ROR1-STAM1 interaction required for HRS-STAM1 binding. 36 (a) IP-WB analysis showing impaired association of ROR1 with HRS, but not CAVIN1, in NCI-H1975 cells following STAM1 knockdown. Cell lysates were harvested at 24 hours after siSTAM1 transfection, when no obvious siSTAM1-induced reduction of HRS expression was seen. (b) Immunofluorescence analysis showing markedly impaired colocalization of ROR1 and HRS induced by STAM1 knockdown. Scale bar, 30 μm. (c) The proline-rich

domain of ROR1 was demonstrated as the STAM1-binding region in IP-WB analysis with various ROR1 deletion mutants. (d) IP-WB analysis showed an impaired association of HRS with STAM1 in ROR1-ΔPm-reconstituted NCI-H1975 cells. TF, transfectant (e) Immunofluorescence analysis indicated significant colocalization of HRS with LAMP-1 in ROR1-ΔPm-reconstituted NCI-H1975 cells. Scale bar, 30 μm.

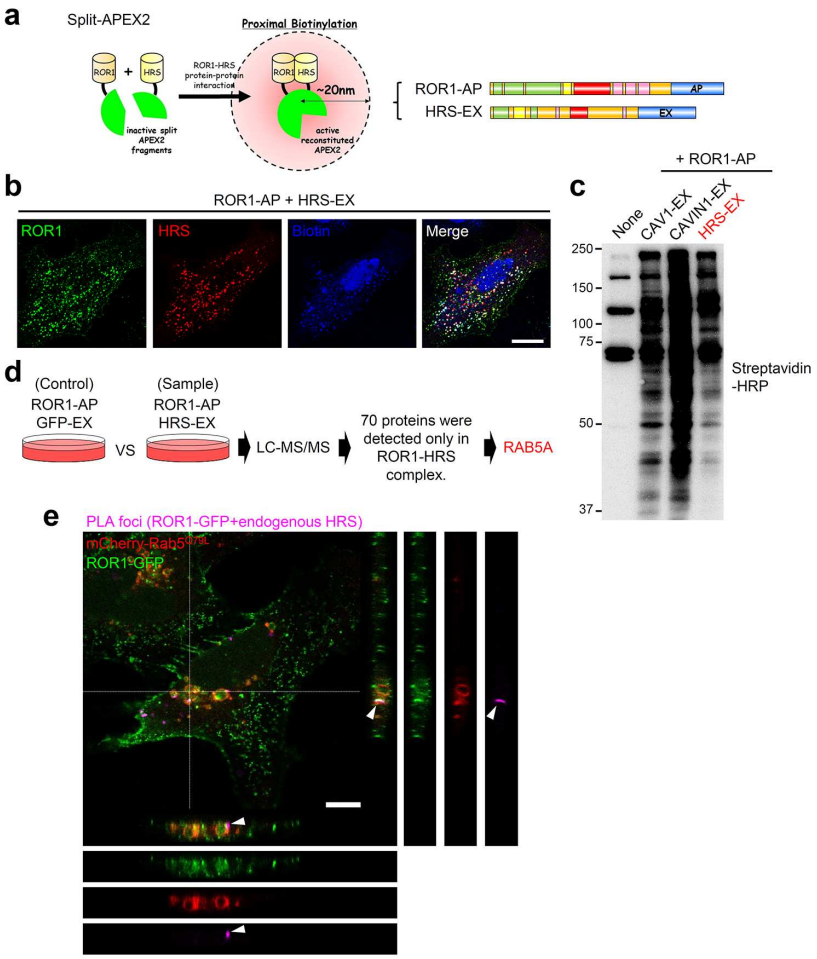

Figure 6

Figure 6

Identification of Rab5 as ROR1-HRS binding protein. (a) Schematic overview of split-APEX2. Two inactive fragments have an ability to reconstitute resulting in active peroxidase when driven together by ROR1-HRS interaction. See Supplementary Fig 4a for a schematic overview regarding split-APEX2 testing of ROR1- STAM1. (b) Biotin labeling was examined using confocal imaging. HeLa cells were transfected with ROR1-AP and HRS-EX, then biotin labeling was initiated with H2O2 following biotin-phenol incubation. Scale bar, 30 μm. See Supplementary Fig 4b for findings regarding ROR1-STAM1. (c) WB analysis was used to test biotin labeling in live cells. Cells were treated as noted in (b). Whole cell lysates were resolved by SDS-PAGE and tested for biotinylated proteins using streptavidin-HRP. See Supplementary Fig 4c for findings regarding ROR1-STAM1. (d) Schematic diagram of strategy for use of split-APEX2 system and LC-MS/MS analysis. 70 proteins were identified only in ROR1-AP- and HRS-EXtransfected HeLa cells. See Supplementary Fig 4d for findings regarding ROR1-STAM1. (e) PLA assays were conducted using mouse anti-GFP and rabbit anti-HRS antibodies. Arrowheads indicate purple foci representing ROR1 in close proximity with HRS in the limiting membrane of Rab5-induced MVEs. Images shown are three-dimensional reconstructions from a series of confocal Z-stack images. Scale bar, 30 μm.

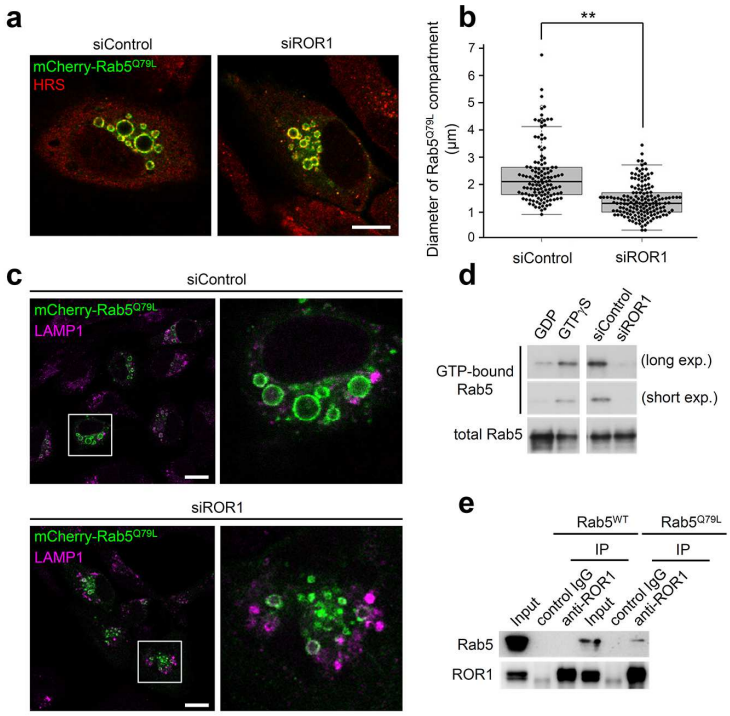

Figure 7

Figure 7

ROR1 required for formation of Rab5-induced MVEs. (a) Effect of ROR1 deletion on Rab5Q79L-induced MVE formation. HeLa cells were treated with siControl or siROR1, then transfected with mCherry-Rab5Q79L. Cells were fixed and examined using confocal microscopy. Images shown are three-dimensional reconstructions from a series of confocal Z-stack images. Scale bar, 30 μm. (b) Quantification of diameters of Rab5Q79L-induced MVEs. Findings shown in (a) indicating endosome

diameter were determined using the line tool of the Image J software package. Lines represent the median, and boxes show the 25th and 75th percentiles of endosome diameters in siControl- and siROR1-treated cells. Whiskers indicate SD. A total of 158 endosomes (siControl) and 124 endosomes (siROR1) from each 11 cells were analyzed. Data were analyzed using Welch's two sample t-test (**P<0.001). (c) Confocal imaging of siROR1-treated HeLa cells showed Rab5Q79L-induced MVEs to be very small, with those structures surrounded by LAMP-1- positive vesicles. Scale bar, 30 μm. (d) ROR1 knockdown reduced GTP-bound Rab5. NCIH1975 cells were transfected with siControl or siROR1, then processed for total protein extraction followed by an Rab5 activity assay, as described in Methods. (e) IP-WB analysis showing association between ROR1 and GTP-bound Rab5 in Rab5WT- and Rab5Q79Ltransfected NCI-H1975 cells.

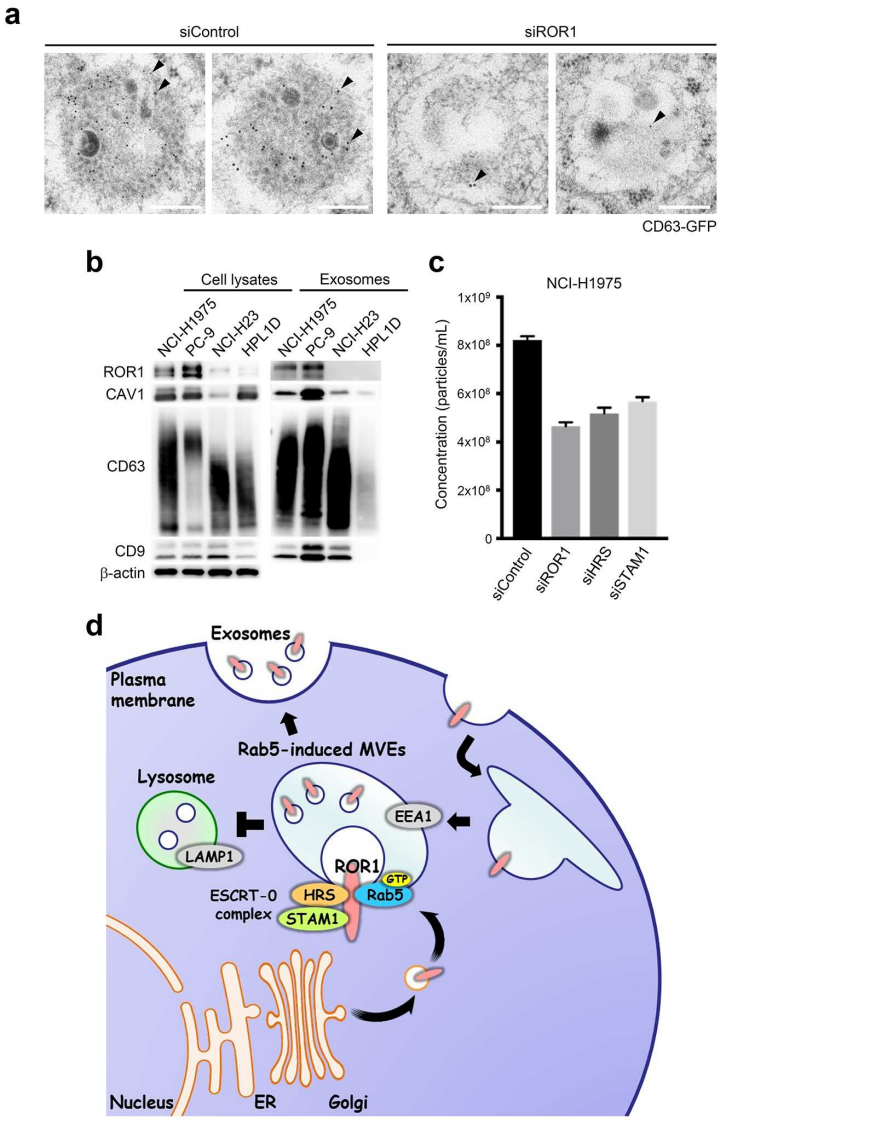

Figure 8

Figure 8

ROR1 depletion inhibited formation of CD63-positive MVEs and reduced exosome release. (a) Representative results of immunoelectron microscopy. After immunogold labeling of cryosections using antibodies against GFP, HeLa cells expressing CD63-GFP were analyzed by electron microscopy. CD63-GFP, indicated by arrowheads, was found localized in ILVs of MVEs in siControl-treated cells. In contrast, siROR1-treated cells showed only CD63-GFP in that area, possibly a vestige of MVE. Scale bar, 200 nm.

(b) Purification of exosomes from conditioned media of cancer cell lines was performed by sequential centrifugation. Whole-cell lysates of NCI-H1975, PC-9, and NCI-H23 lung cancer cell lines, as well as HPL1D human peripheral lung epithelial cells were subjected to WB analysis with the indicated antibodies. The total exosome fraction isolated from conditioned media of the cell lines by sequential centrifugation was also subjected to WB analysis. (c) NCI-H1975 cells were transfected with siControl, siROR1, siHRS, or siSTAM1, then conditioned medium samples were subjected to exosome preparation, followed by an NTA assay for quantitative measurement of isolated exosome particles. Values reflect the mean ± SD of three independent experiments. (d) Schematic diagram of proposed model showing how ROR1 sustains MVE formation and exosome biogenesis. ROR1 facilitates the interaction of HRS with STAM1 at the limiting membrane of Rab5-induced endosomes, which results in sustained MVEs formation and exosome biogenesis via its scaffold function for HRS and STAM1 in human cancer cells.

Supplementary Files

This is a list of supplementary files associated with this preprint. Click to download.

- SupplementaryFigures.pdf
- SupplementaryTable1.pdf
- ncommslifescienceschecklist.pdf